QUARTERLY JOURNAL OF THE ROYAL METEOROLOGICAL SOCIETY
Q. J. R. Meteorol. Soc. **134**: 147–163 (2008)
Published online 7 January 2008 in Wiley InterScience
(www.interscience.wiley.com) DOI: 10.1002/qj.193

Influence of local and remote sea surface temperatures on precipitation as inferred from changes in boundary-layer moisture convergence and moist thermodynamics over global oceans†

Y. C. Sud,* G. K. Walker, Y. P. Zhou and W. K.-M. Lau
Laboratory for Atmospheres, NASA Goddard Space Flight Center, Greenbelt, Maryland, USA

ABSTRACT: A comprehensive method of estimating the influences of local versus remote sea surface temperatures (SSTs) on precipitation is developed. The method was applied to two ten-year simulations made with a general circulation model (GCM) and forced with prescribed SSTs. The simulation period spanned from 1 January 1982 to 31 December 1991. The first simulation (called Cs) was forced with naturally varying SSTs taken from the analysis of observations and the second simulation (called Cc) was forced with monthly mean climatology of SSTs used in Cs. Monthly data of evaporation, precipitation, mean vertical velocity and atmospheric moisture convergence were binned by 1 °C SST intervals and plotted as bin means and within-bin standard deviations. The plots showed that (i) binning captured the averaged trend of SST influences on the monthly fields, but with large standard deviations; (ii) all bin-averaged SST dependences were remarkably similar in the two simulations as well as in the single El Niño Southern Oscillation year of 1987; (iii) evaporation increased monotonically with SST up to about 27 °C after which it plateaued; and (iv) precipitation correlated much more with the vertical velocity than with the local SST.

Monthly precipitation fields were doubly binned with respect to SSTs and boundary-layer moisture convergence (BLqC); data binned in this way were used to compute the partial derivatives of precipitation with respect to SST and BLqC. Together with the total rate of change of BLqC with local SSTs, the rate of change of precipitation with local SST was computed. The remaining precipitation differences were lumped together as all other remote effects. Simulation Cc was used to infer the natural variability of the precipitation required for the statistical significance of the local SST and/or remotely caused changes in precipitation. This analysis categorized all precipitation anomalies into four types: (i) where the local SST influences were significant, (ii) where the remote SSTs influences were significant, (iii) where both influences were significant, and (iv) where the natural variability was larger than both influences. Most of the precipitation responses to SSTs were as expected, while their seasonal behaviour revealed that local SSTs contribute to a number of features of the Intertropical Convergence Zone (ITCZ) including the double ITCZ in March–April–May. Published in 2008 by John Wiley & Sons, Ltd.

KEY WORDS GCM; SST; precipitation; physical dynamic responses

Received 22 March 2007; Revised 7 November 2007; Accepted 9 November 2007

1. Introduction

The annual cycles of global sea surface temperature (SST) fields and solar irradiation are central to the seasonally evolving quasi-stationary structures of the atmospheric circulation and precipitation. Rind and Rossow (1984) found that, in their model simulations, SST forcing was sufficient to maintain the basic structures of the Hadley and Walker circulations, irrespective of the solar irradiation. Their study has established the pivotal role of SSTs for maintaining the fundamental structures of the global circulation. Moreover, it is well known that the intensely rainy areas of the tropical oceans follow the high SSTs (e.g. Giannini *et al.*, 2001) during the warm and cold phases of El Niño Southern Oscillation (ENSO). Dozens of studies employing observed and model-simulated data have shown how SST anomalies drive the precipitation anomalies in the tropics (e.g. Su *et al.*, 2001; Chen, 2005). It is also well known that ENSO-induced changes in tropical circulation affect weather and climate of mid and high latitudes by modulating the quasi-stationary wave trains. Evidently, *in situ* SSTs, local SST gradients, and large-scale SST fields are important for the precipitation; therefore distinguishing their influences on precipitation is vital for understanding the behaviour of precipitation anomalies on inter- and intra-annual time-scales. On the other hand, some recent work showed that regional SST anomalies can be forced by circulation anomalies and emphasized the importance

* Correspondence to: Y. C. Sud, NASA Goddard Space Flight Center, Laboratory for Atmospheres, Greenbelt 20771, Maryland, USA.
E-mail: sud@climate.gsfc.nasa.gov
† This article is a U.S. Government work and is in the public domain in the U.S.A.

of two-way interactions, better represented in coupled models, for realistic simulation of the air–sea interactions (e.g. Wang *et al*., 2005).

The high nonlinearity between dynamics and thermodynamics limits us to analyze only those scenarios in which linearity can be assumed, i.e. where SST perturbations at individual grid cells are not so large as to alter substantially the basic structure of the mean monthly circulation and precipitation. Several aspects of relationships between atmospheric circulation and SST have been examined in both atmospheric and oceanic circulation scenarios using simulated data as well as observations (e.g. Yu *et al*., 1991; Harrison and Craig, 1993; Bony *et al*., 1997; Lau *et al*., 1997; Del Genio and Kovari, 2002; Lohmann *et al*., 2002; Seager *et al*., 2003; Gushchina *et al*., 2006; Lin *et al*., 2006). Specifically, Del Genio and Kovari (2002) examined the relationships between the rain-rate and storm radius and related them to key atmospheric diagnostics and SSTs following a regression technique. Lin *et al*. (2006) analyzed the increase in boundary-layer moisture convergence (BLqC) and precipitation efficiency as a function of local SST for tropical deep-convective systems and thereby demonstrated the need to include the BLqC contributions to the SST–precipitation relationship. Bony *et al*. (1997) illustrated use of SST and vertical velocity binning to differentiate between local and remote SST effects on precipitation in the Tropics, while Lau *et al*. (1997) used the 200 hPa divergence fields for categorizing different convective scenarios. Nevertheless, a comprehensive methodology for understanding the influences of local versus remote SSTs on precipitation remains elusive. Our study aims to fulfill the above need. A multi-variable data analysis employing two partial derivatives of doubly binned fields was instituted to distinguish the influence of local SSTs on local precipitation due to changes in atmospheric column thermodynamics and BLqC; the remaining dynamic effects (namely remote SSTs, clouds, cloud-radiative and hydrologic forcings) were obtained as differences between the total precipitation and local-SST-modulated precipitation. The methodology is limited to small SST perturbations otherwise the nonlinearity of SST–dynamics interactions voids the assumption of an analysis using partial derivatives.

The 4-Dimensional Data Assimilation (4DDA) can provide the observation-quality data for the proposed analysis; however, the 4DDA process infuses substantial data pollution of the vertical velocity and precipitation fields; consequently, 4DDA data of these two fields is unsatisfactory for our study. Moreover, data assimilation involves resolving mismatches between observed and simulated data fields because of (a) differences in time- and space-scales of observations and grid-mean fields, and (b) discernible biases of GCMs (the centrepiece of all 4DDA systems) that interact with the assimilated data. Alternatively, free-running GCMs yield internally consistent data and also allow controlled simulations to better isolate the influence of different physical interactions. Nevertheless, if the chosen GCM has large biases, its simulations would not be as credible as observations would be. In the multi-model study of Koster *et al*. (2004), different GCMs produced widely different precipitation response(s) to soil moisture anomalies. Naturally, one faces the proverbial dilemma – how to distinguish between the model characteristics and the true behaviour of the atmosphere. We feel that, if observations are used as a guide, model-simulated data can provide reasonable insight into the response of precipitation to SST changes. We chose the model simulation route and employed one of the operational GCMs at Goddard Space Flight Center (GSFC) for the investigation. Regardless, our inferences are data dependent and may change if better data from coupled ocean–atmosphere models or 4DDA analyses become available.

The Goddard finite volume GCM (called fvGCM or GEOS4 GCM) was used for the present study. It uses finite-volume hydrodynamics, and National Center for Atmospheric Research (NCAR) land and boundary-layer physics. It has been used at GSFC for weather and climate simulation studies extensively (e.g. Betts *et al*., 2003; Kim *et al*., 2006; Sud *et al*., 2006). The model has very reasonable monthly circulation climatology (Chang *et al*., 2001), but then it also has some discernible biases in the regional precipitation patterns. Our version of fvGCM uses NASA/GSFC indigenous cloud physics and radiation schemes (see Section 2). The overall structure of the simulated precipitation is quite reasonable despite some biases in the magnitudes (see Section 4.1). The simulated seasonal cycles of precipitation (not shown) also had several remarkable similarities with the corresponding observations, even though the diurnal cycle of precipitation over the oceans has large biases. We also need the intrinsic variability of the simulated precipitation to assess the statistical significance of the local and remote SSTs on precipitation; these are easily inferred from climatological SST simulations.

2. Model description

The fvGCM has a finite-volume (fv) dynamical core that was extensively evaluated by Lin and Rood (1996) while the theoretical basis of its fv hydrodynamics has been comprehensively discussed by Lin (2004). Initially, the entire GCM physics (Hurrell *et al*., 1998) was from NCAR. Specifically, the land–atmosphere interaction scheme was from NCAR CCM3.6 community model version 2.0 – CLM2 (Community Land Model 2; Hurrell *et al*., 1998). The GCM was initially named fv-NCAR GCM. Its name was changed to fvGCM after extensive tuning of its physics. It was subsequently distinguished as GEOS4 GCM by the Global Modeling and Analysis Office (GMAO) at the GSFC. Microphysics of clouds with a Relaxed Arakawa–Schubert scheme (McRAS; Sud and Walker, 1999a) was included as an option to the original cloud physics. McRAS is structured around the moist convection of the Relaxed Arakawa–Schubert scheme (RAS; Moorthi and Suarez,

1992) but it employs Sundqvist *et al.* (1989) cloud microphysics, Tiedtke (1993) cloud-mass and cloud-water transport algorithms, and Del Genio *et al.* (1996) cloud-top entrainment instability parametrization. McRAS simulates cloud amounts by solving prognostic equations of cloud-mass and cloud-water substance in which cloud and precipitation microphysics remain fully interactive and prognostic for all cloud types, namely stratiform, boundary-layer, and convective. Its algorithms and evaluations have been discussed in papers by Sud and Walker (1999a,b, 2003). McRAS also performed better in the fvGCM (Sud *et al.*, 2006) as well as in an earlier version of NCAR GCM (Maloney and Hartman, 2001; Maloney, 2002; Sud *et al.*, 2006), particularly in the Tropics.

The model's radiative flux transfer schemes (Chou and Suarez, 1994) were developed and extensively validated at GSFC. Its several upgraded algorithms are discussed in Chou *et al.* (1998, 1999). The schemes perform radiative transfer calculations using cloud water, water vapour and air temperature fields generated and/or modified by McRAS. The fv-NCAR GCM modified in this way will be called fvGCM2 hereafter. The model resolution employed in the simulations is 1.0° latitude $\times$1.25° longitude, with 55 vertical layers. The model covers the atmosphere from the ground surface to an altitude of approximately 75 km. More details of the model's cloud physics can be found in the papers referenced above.

3. Data and methodology

3.1. Model simulations

All model simulations were performed with the fvGCM2 and forced with the analyzed monthly SST and sea-ice data fields provided by Rayner *et al.* (2002). The monthly SST data were linearly interpolated to obtain daily SST fields. The initial soil moisture fields were taken from a 47-year 'spin-up' of the standard fvGCM integration with several months of daily soil moisture updates using observed circulation data. (This procedure may not provide observation-quality analysis, but it is a reasonable alternative to performing an extensive soil moisture analysis with a crude land-hydrology data assimilation system using *in situ* observations that in all likelihood would be inconsistent with the GCM's horizontal resolution and/or land hydrology and physics of its biospheric processes.) We needed at least 10-year integrations to encompass the different phases of the multiple equilibria and/or to capture various modes of chaotic variability of the atmosphere. Hence we made two model integrations covering the 10-year period, 1 January 1982 to 31 December 1991. The first integration (named Cs) was forced with the naturally varying SSTs, and the second integration (named Cc) was forced with the 10-year mean SSTs that contained the mean annual cycle but without the interannual variability. The biosphere, with its phenology and morphology, was also prescribed from monthly data. In the upper atmosphere, the ozone fields were climatological and prescribed as monthly data. All other physical interactions, e.g. clouds and precipitation, cloud–radiation interaction, soil moisture in association with land hydrology, as well as the simulated circulation, were prognostic and fully interactive. A number of studies, going back to Waliser's (1996) discovery of hot spots over tropical oceans, have shown that SST anomalies can be caused by feedback response to persistent quasi-stationary circulation anomalies (Fu *et al.*, 2007); however, prescribed-SST simulations circumvent the additional complexities of fully prognostic SSTs. Clearly, prescribed-SST simulations would be unable to respond to a myriad of circulation-forced SST anomalies that emerge due to variations in mixed-layer humidity, or winds, or air–sea contrast for otherwise similar descent in the Tropics (Su and Neelin, 2002), warm or cold advection over the ocean (Cayan, 1992) and short-time-scale cloudiness variations influencing the net radiation into the ocean. On the other hand, many simulations forced with the prescribed SSTs have produced quite realistic relationships between precipitation and SST. For example, Peña *et al.* (2004) showed that most of the long-lasting atmospheric anomalies are locally coupled with SST anomalies. Thus, lack of ocean–atmosphere coupling may not be critical for the outcome of our study as long as the SST-forced circulation and its dependent precipitation fields are well simulated. The most relevant criterion is the GCM's ability to simulate the statistics of moisture convergence and precipitation in response to global SSTs whose partial derivatives with SST are central to our analysis. Such statistics of the fvGCM have been analyzed by Chang *et al.* (2001).

3.2. Methodology

Two sources of moisture for precipitation are surface evaporation, E_{ss}, and horizontal moisture convergence,

$$-\int_{p_s}^{p_t} \nabla_p \cdot V_h q \, dp,$$

where V_h is the horizontal velocity, q is water vapour mixing ratio and p_s and p_t are the pressures at the surface and the top of the troposphere. A small fraction of the condensate is stored as cloud water but, on a monthly time-scale, changes in cloud-water storage can be ignored. One can subdivide the column moisture convergence into two parts, one associated with the mass convergence,

$$-\int_{p_s}^{p_t} q \nabla_p \cdot V_h \, dp \text{ (the so-called primary term)},$$

the other related to the humidity gradient,

$$-\int_{p_s}^{p_t} V_h \cdot \nabla_p q \, dp \text{ (the so-called complementary term)}.$$

Both terms contain the dependence of moisture convergence,

$$-\int_{p_s}^{p_t} \nabla_p \cdot V_h q \, dp,$$

on SST and humidity fields. On monthly time-scales, the precipitation, P and its perturbation δP can be expressed by

$$\delta P = \frac{\partial P}{\partial E_{ss}} \delta E_{ss} + \frac{\partial P}{\partial M_b} \delta M_b + \frac{\partial P}{\partial M_t} \delta M_t, \quad (1)$$

where M_b and M_t are moisture flux convergences in the boundary-layer and upper regions of the column atmosphere. This partitioning is physically defensible. Almost all clouds rely on boundary-layer moisture convergence; large-scale clouds in midlatitudes, often associated with low pressure with air-mass ascent in the planetary boundary layer (PBL), form in-cloud condensation and precipitation, while convective clouds rely on water vapour from the cloud sub-layer (or the mixed layer) via the cloud-base mass flux (Moorthi and Suarez, 1992). Our goal is to determine each term of Equation (1) to isolate the relative influences of the local and non-local SSTs on precipitation. The surface evaporation change δE_{ss} is primarily local-SST forced because the PBL buoyant stability, winds, humidity gradients in the vertical, and ocean surface roughness can be assumed invariant. Hence, we write

$$\frac{\partial P}{\partial E_{ss}} \delta E_{ss} = \frac{\partial P}{\partial T_{ss}} \delta T_{ss}. \quad (2)$$

Using (2) in a model with several layers in the PBL and aloft regions, we recast Equation (1) as

$$\frac{dP}{dT_{ss}} = \frac{\partial P}{\partial T_{ss}} + \sum_{PBL} \frac{\partial P}{\partial M_b} \frac{dM_b}{dT_{ss}} + \sum_{Top} \frac{\partial P}{\partial M_t} \frac{dM_t}{dT_{ss}}. \quad (3)$$

Often dM_t/dT_{ss} is much smaller than dM_b/dT_{ss} because of its remoteness from the ocean surface and has much lower saturation water vapour pressure at lower temperatures above the PBL. Moreover, the top layers contain a mix of converging and diverging air masses. Our diagnostics based on the GCM-simulated data confirmed the reasonableness of this assumption; hence the contribution of the term dM_t/dT_{ss} was ignored. On summing up dM_b/dT_{ss} through the PBL height and introducing ambient temperature T_{amb} into the chain rule applied to derivatives being multiplied, we have

$$\sum_{PBL} \frac{dM_b}{dT_{ss}} = \frac{d}{dT_{amb}} \left[-\left\{ \nabla_b \cdot \sum_{PBL} V_h q_b \right\} \right] \frac{dT_{amb}}{dT_{ss}} \quad (4a)$$

$$= \left[-\sum_{PBL} \left\{ \nabla_b \cdot \frac{dV_h}{dT_{amb}} q_b \right\} - \sum_{PBL} \left\{ \nabla_b \cdot V_h \frac{dq_b}{dT_{amb}} \right\} \right] \frac{dT_{amb}}{dT_{ss}}, \quad (4b)$$

where ∇_b, V_h, q_b are the Del operator, horizontal wind velocity, and specific humidity in the PBL. The summation reflects the fact that the PBL covers several model layers. If we assume that the monthly relative humidity of the PBL over the ocean does not change much due to SST perturbations, and approximate the saturation vapour pressure, q^*, by $q^* = C \exp(A - B/T)$, to get $dq^*/dT = q^* B/T^2$, and also define $dT_{amb}/dT_{ss} = \alpha$, we obtain

$$\frac{dq}{dT_{ss}} = RH \frac{dq^*}{dT_{amb}} \left(\frac{dT_{amb}}{dT_{ss}} \right) \approx \frac{B\, q}{T_{amb}^2} \alpha, \quad (5a)$$

and that modifies (4b) to

$$\sum_{PBL} \frac{dM_b}{dT_{ss}} = \left[-\sum_{PBL} \left\{ \nabla_b \cdot \frac{dV_h}{dT_{amb}} q_b \right\} - \sum_{PBL} \left\{ (\nabla_b \cdot V_h q_b) \frac{B}{T_{amb}^2} \right\} \right] \alpha. \quad (5b)$$

Invoking an additional assumption (supported by the simulated data of Cc and Cs) that horizontal velocity is little affected by the local SST perturbation, we can drop the first term of the right-hand side and reduce Equation (5b) to:

$$\sum_{PBL} \frac{dM_b}{dT_{ss}} = -\sum_{PBL} \left\{ (\nabla_b \cdot V_h q_b) \frac{B}{T_{amb}^2} \right\} \alpha. \quad (6)$$

Equation (6) was used to compute $\sum dM_b/dT_{ss}$. If the partial derivatives $\partial P/\partial T_{ss}$ and, $\partial P/\partial M_b$ are obtained from doubly binned precipitation data as a function of T_{ss} and M_b, we have all the terms needed for computing the thermodynamic influence of local SSTs on precipitation. The dynamic or remote effects are simply equal to the difference between the simulated changes in total precipitation in the Cs integration minus the computed thermodynamic influence of the local SST at every grid cell.

4. Results

4.1. SST and precipitation fields

The 2D contour plots of 10-year mean precipitation fields are shown along with the corresponding prescribed-SST fields (background patterns) for observations (Figure 1(a); Huffman *et al.*, 1997) and for Cs simulations (Figure 1(b)). The similarity between the simulated and the observed precipitation fields is quite reasonable. The precipitation patterns are quite similar although the precipitation intensities have some discernible biases. Only in the Tropics are the isopleths of SST parallel to the isopleths of precipitation. The intersection angle between them suggests the relative importance of remote effects of SSTs. Although we do not show how SST variations led to corresponding precipitation variations in

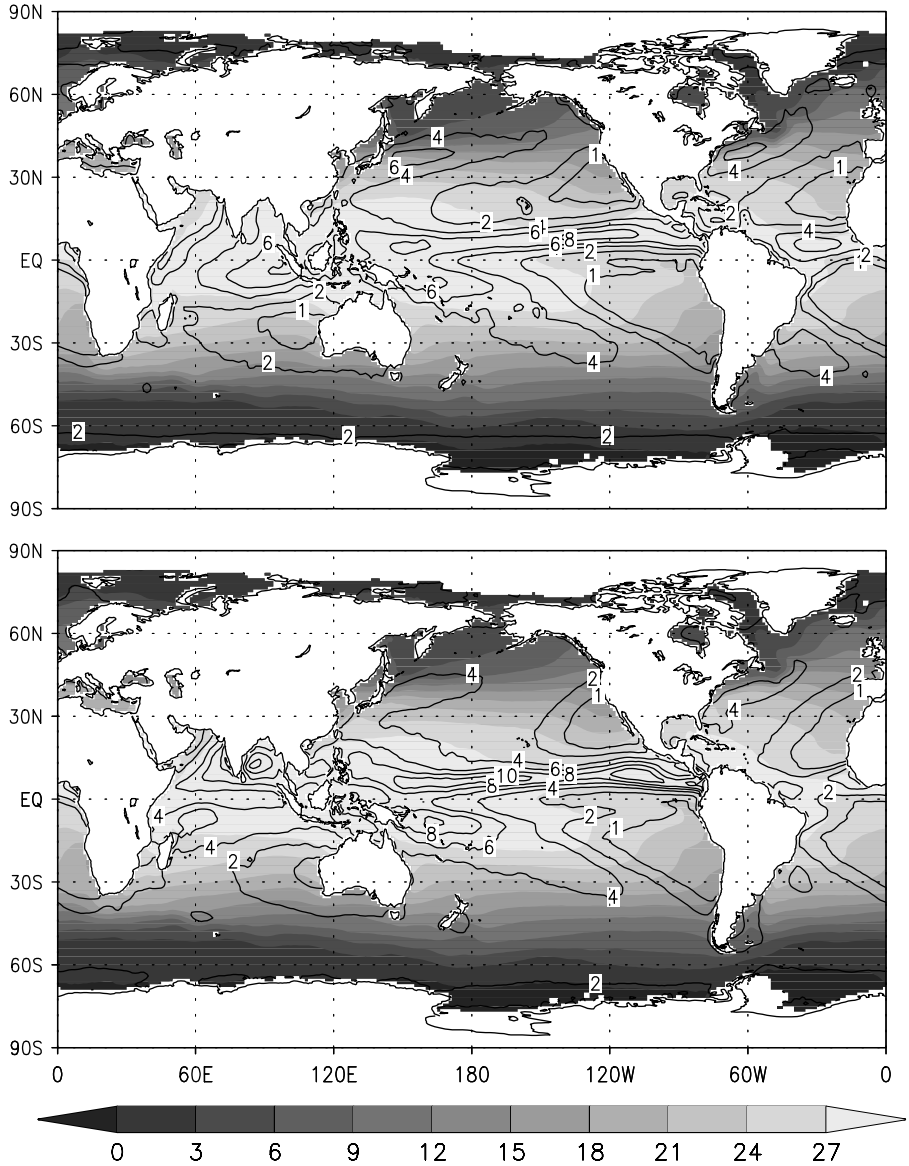

Figure 1. Composite plots of prescribed SST (°C; shading, see key) and precipitation fields (mm d^{-1}; contours) shown as 10-year averages: (a) GPCP estimates and (b) GCM simulated.

different regions, the well-known relationships between tropical SSTs and tropical precipitation was evident in the comparisons. All the SST–precipitation relationships are based on the Cs data; hence realism of its precipitation climatology is vital for the accuracy of our inferences. We probe into various aspects of SST–precipitation relationships in the subsections that follow.

4.2. Binned evaporation, precipitation, vertical velocity and moisture convergence

The 10-year monthly data for evaporation, precipitation, vertical velocity, and BLqC were binned by 1 °C SST intervals and plotted. Figures 2(a)–(d) show the bin-mean values of each of the four fields as a function of SST along with an envelope of standard deviation (shown only for the Cs simulation). Similar means and standard deviation were produced for Cc simulation as well as for a single ENSO year (1987) (called Ce). The standard deviations of the Cc and Ce simulations (not shown) were very similar to those of the Cs simulation. Even the bin-averaged values of each of the four quantities in the Cc and Ce were very similar to those of Cs except for SSTs larger than 29 °C (see Section 4.3 for discussion). The large variations in the monthly means can be due to remote contributions and/or intrinsic variability. It is well known that there is very little precipitation over the hot spots (Waliser, 1996), such as are found in the tropical Indian Ocean. Consequently, the bin-averaged precipitation decreases for SST >29 °C where our simulation data also show more divergent and less convergent bin members. Such a feature was also seen in the Lin *et al*. (2006) study. The sample size for the highest SST bin of the climatological SST simulation was also small. Hence the differences between the Cs and Ce simulations for SST >29 °C may be spurious (Section 4.3).

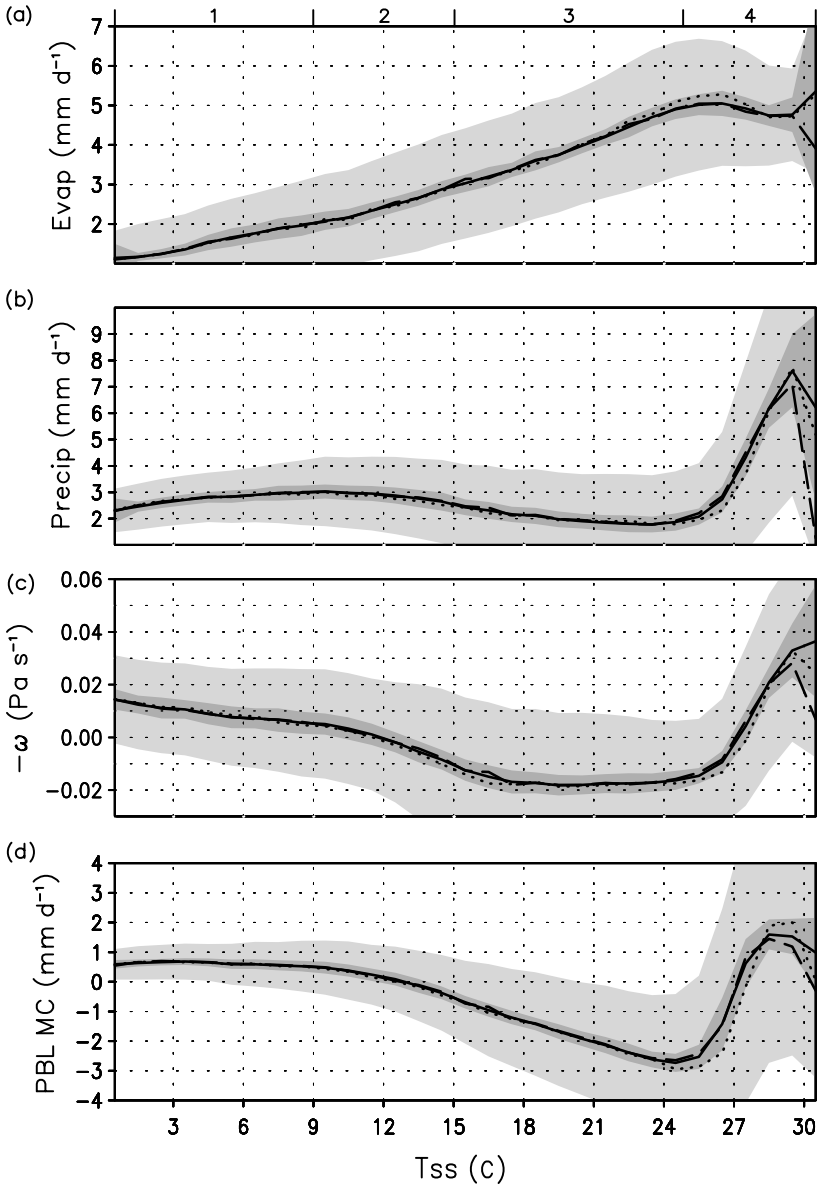

Figure 2. 10-year mean GCM-simulated fields of (a) evaporation, (b) precipitation, (c) 850–300 hPa upward vertical velocity ($-\omega$), and (d) PBL moisture convergence (BLqC or MC), binned by SST. The simulations are Cc (long dash), Ce (dotted), and Cs (solid), with Cs standard deviation shown by light shading. Darker shading represents all 10 years of binned data.

Furthermore, the bin-averaged monthly evaporation increases monotonically with SST up to about 26 °C; after which it plateaus (or even reduces) for higher-SST regimes (Figure 2(a)). This occurs primarily in the rainy regions. Regions of reduced evaporation emerge in strongly converging humid regions, e.g. the warm pool. In these regions, the wind speed is relatively small whereas the near-surface relative humidity is high, both of which reduce evaporation. Chou *et al.* (2005) noted similar SST–evaporation relationships in their analysis of observations and found that its primary cause is low wind speed. In fact, inability of moist convection to remove water vapour efficiently from the boundary layer also contributes to this outcome. According to Larson and Hartmann (2003a,b), cooling by radiation in the Tropics is the primary driver of moist convection that must draw the humid air from the cloud sub-layer and deliver condensation heating to mitigate the radiative cooling. Since converging air at these temperatures is sufficiently humid, surface evaporation serves a merely complementary role of a water vapour supplier to the PBL in case its humidity drops, e.g. by dry downdraughts. Such PBL moisture constrains put an upper limit on the amount of evaporation in high-SST regions of the Tropics. Indeed, it would be even smaller, but for the episodic dynamics, sudden wind bursts and convective downdraughts leading to drying episodes.

The bin-averaged precipitation regimes are associated with four different dynamic regimes. In high latitudes, with SST range 0–9 °C, the precipitation increases only slightly with SST (Figure 2(b)). In the SST range 9–24 °C, the precipitation decrease with SST is mainly associated with the sinking branch of the Hadley and Ferrel circulation(s). For still larger SSTs, between 24

and 29 °C, the precipitation increases very sharply with SST in association with the relative increase of moisture convergence. Finally, for SSTs higher than 29 °C, the precipitation decreases again. The precipitation patterns show a good correlation with the bin-averaged vertical velocity (Figure 2(c)), except for the highest temperature bin in the Cs simulation. One sees that positive correlation of SST and precipitation corresponds to positive 850–300 hPa mean upward vertical velocity and the rising branches of the Hadley and Ferrel cells, while the negative correlation of SST and precipitation corresponds to negative 850–300 hPa mean vertical velocity and the sinking branches of Hadley and Ferrel circulations. In regions of large-scale subsidence, there is high surface evaporation and moisture divergence (Figure 2(d)). The tropical regime of the Hadley circulation is associated with relatively smaller Coriolis force and abundant moisture supply; it produces large condensation heating that in turn draws extra tropical moisture due to thermally induced convergence. The moisture loss and associated precipitation reduction in the subsidence regions is an outcome of the ability of the Tropics to utilize the condensation heating. The highest SST bin with highest evaporation and highest upward vertical velocity in the PBL has reduced precipitation. The explanation of this is as follows. This SST bin has significant contribution from the Red Sea and Persian Gulf regions where there is copious evaporation. The air aloft is in descent while the near-surface dry desert air is warm (low relative humidity and high evaporation) and in a thermal low delivering rising motion to the PBL. Together they cause mixing of the PBL and dry diverging air to carry the moisture out and suppress clouds and precipitation. This happens both in nature as well as in our model, which makes the region unique. Overall, large-scale organization of circulation patterns that are coupled to large-scale SST patterns are ubiquitous in the Tropics. These structures are manifest through negative correlations between SST and vertical velocity or precipitation in the medium-range SST of the extratropical regions.

Strong SST–precipitation association occurs at SST ~26 °C where the bin-averaged subsidence motion (seen at lower SSTs) sharply changes into the bin-averaged rising motion. Clearly, larger moist-static energy associated with higher SSTs triggers moist convection. This is roughly the regime where deep convection ensues with significant condensation of the converging moisture causing the precipitation to exceed the evaporation. Its characteristic behaviour was discussed by Sud *et al.* (1999) using data from the Tropical Ocean–Global Atmosphere Coupled Ocean–Atmosphere Response Experiment (TOGA–COARE) and first principles of moist convection (also see Zhang, 1993). Here, SST-binned PBL moisture convergence closely corresponds to vertical velocity. The increase of the moisture convergence for SST between 26 and 29 °C is associated with convergence in the Intertropical Convergence Zone/South Pacific Convergence Zone (ITCZ/SPCZ) and is partly due to the increase of PBL moisture content also noted by Lin *et al.* (2006). The model's response of zonal precipitation to SSTs is in good agreement with Zhang (1993), which gives confidence in the realism of our simulations.

Both large standard deviation and large reduction in three of the four fields (Figures 2(b)–(d)) near the highest SSTs reflect non-alignment of only a few high-SST cells with the atmospheric dynamics associated with large-scale circulation (see Section 4.3). Waliser (1996) suggested that solar heating in non-precipitating regions is the primary cause of hot spots; however, in the prescribed SST simulations, there is no cloudiness–solar radiation–SST feedback, whereas we still find reduced precipitation for SSTs larger than 29 °C. In our prescribed SST simulations, it represents the response of the scattered warm regions to the atmospheric circulation systems due to their geophysical juxtaposition in which large-scale circulation systems are often out of phase with the highest SSTs.

4.3. Grid-cell counts in SST bins subdivided by BLqC

Figure 3 shows a histogram of the population of grid cells in 2 °C SST bins. Each SST bin is further subdivided into 10 sections denoted by reducing shading density (see bar-scale) for increasing moisture convergence. Each of the 45 500 ocean grid cells of the GCM provided 120 data points (12 months × 10 years). Thus, we have a total of 5.466×10^6 data points occupying 150 bins (i.e. 15 bins to cover the SST range and 10 bins to cover the moisture convergence range from −4 to 6 mm d^{-1}). However, we saw only 345 data points in the highest (29–31 °C) SST bin. This population is very small in comparison to the other bins, as is evident in the histogram. Of these, roughly half the data points

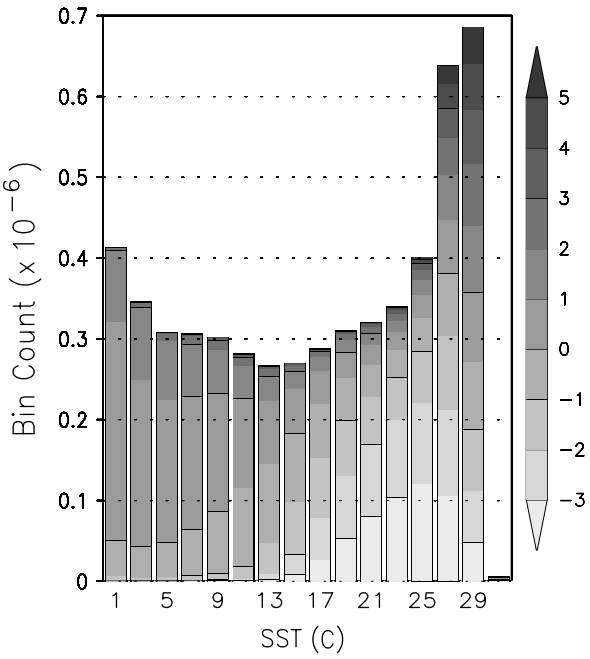

Figure 3. Histogram for total number of grid cells in 10 years of monthly data in each SST bin, which is further subdivided into ten sections for BLqC (shading key, mm d^{-1}).

are in the divergent BLqC regime. We also found that the 29–31 °C SST bin had a large number of grid cells from the Red Sea–Persian Gulf–Gulf of Oman area that experiences strong subsidence with very little rain (see Section 4.2). Thus, this bin is unique. In most of the SST bins in the 19–26 °C range, there is a preponderance of negative BLqC data points, consistent with precipitation decreasing with SST. In short, the bin population as a function of SST and further subdivided on the basis of moisture convergence or divergence provided distinct relationships among SST evaporation, BLqC and precipitation. Even though Cs simulation produced very few hot spots (high SSTs with little rain) in the open oceans, it is argued that hot spots can develop if the SST region is under a divergent circulation with descent and a cloud-free air column enabling the tropical sun to increase the SST below. Potentially, these scenarios can be better simulated with coupled ocean–atmosphere models, in which the coupling enables the SST to increase under cloud-free descent.

4.4. Global evaporation and column moisture convergence

Surface evaporation (Figure 4(a)) and moisture flux convergence in the troposphere (Figure 4(b)) are the primary sources of water vapour for precipitation. The latter is further divided into the primary term due to mass convergence (Figure 4(c)) and the complementary term due to humidity gradient (Figure 4(d)). The similarity of the patterns between the total moisture convergence (Figure 4(b)) and the primary term (Figure 4(c)) shows the dominant role of mass convergence as a moisture source. It naturally leads to a strong relationship between binned precipitation and vertical velocity as delineated by Bony *et al.* (1997). The second term is negative over most ocean areas. It shows that the humidity gradient fields of the tropical and extratropical oceans work as moisture sources for the few intensely precipitating regions such as the ITCZ, the SPCZ and the warm-pool region. The only exception is the cold-tongue region of the Equatorial Eastern Pacific as well as small precipitating regions at high latitudes. This humidity gradient will be enhanced by SST perturbations and was utilized in our analysis of local-SST influence on precipitation.

4.5. Evaporation, PBL moisture convergence (BLqC), and precipitation analysis

Now we examine the doubly binned monthly evaporation, PBL mass convergence (BLmC), and precipitation data by equal intervals of SST and BLqC (Figure 5). The 2 °C interval for the SST bins was adequate for (i) mitigating the influence of SST variations around the monthly mean value because of daily varying SST, and (ii)

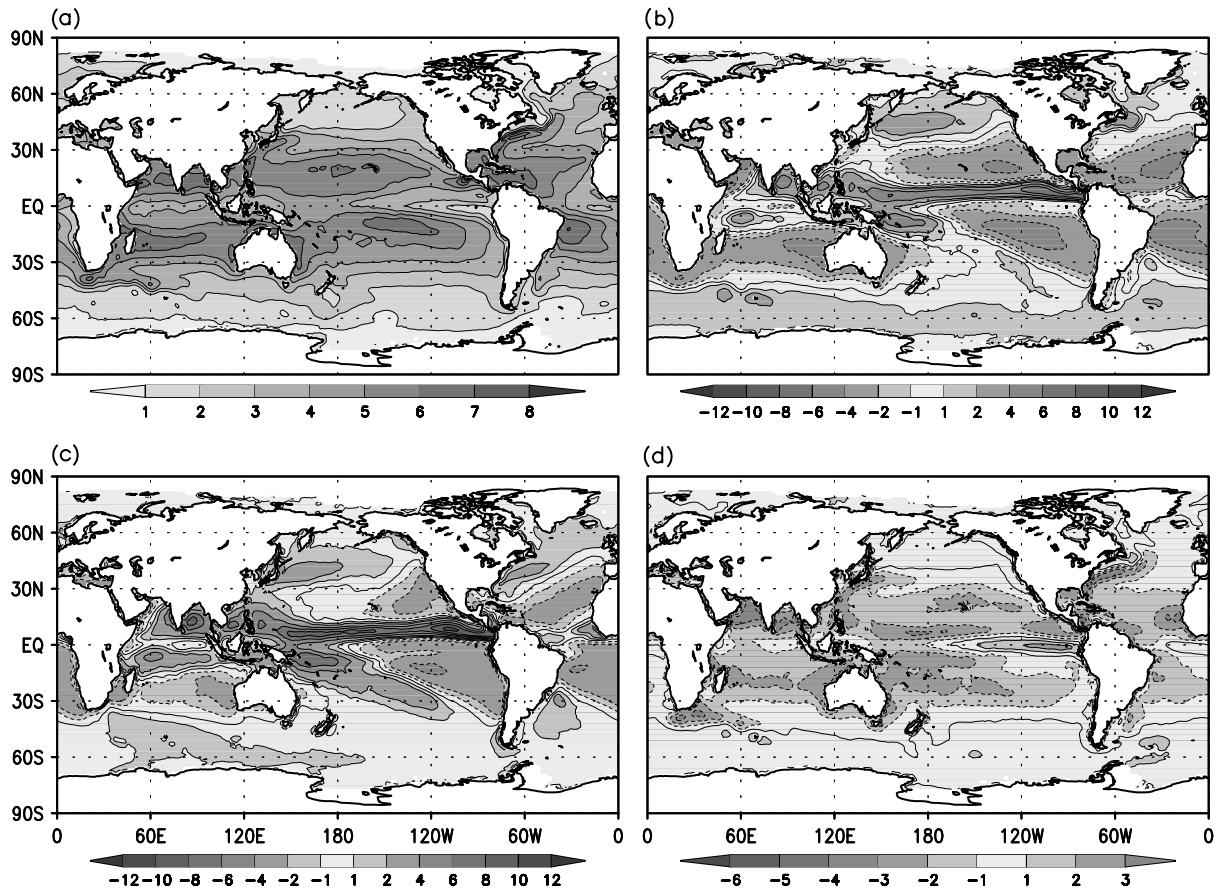

Figure 4. Evaporation and different components of column moisture convergence: (a) oceanic evaporation, (b) $-\int \nabla \cdot V\, q$, (c) $-\int q \nabla \cdot V$, and (d) $-\int V \cdot \nabla q$ of the 10-year simulation. Contours are in mm d^{-1}, and negative contours are dashed.

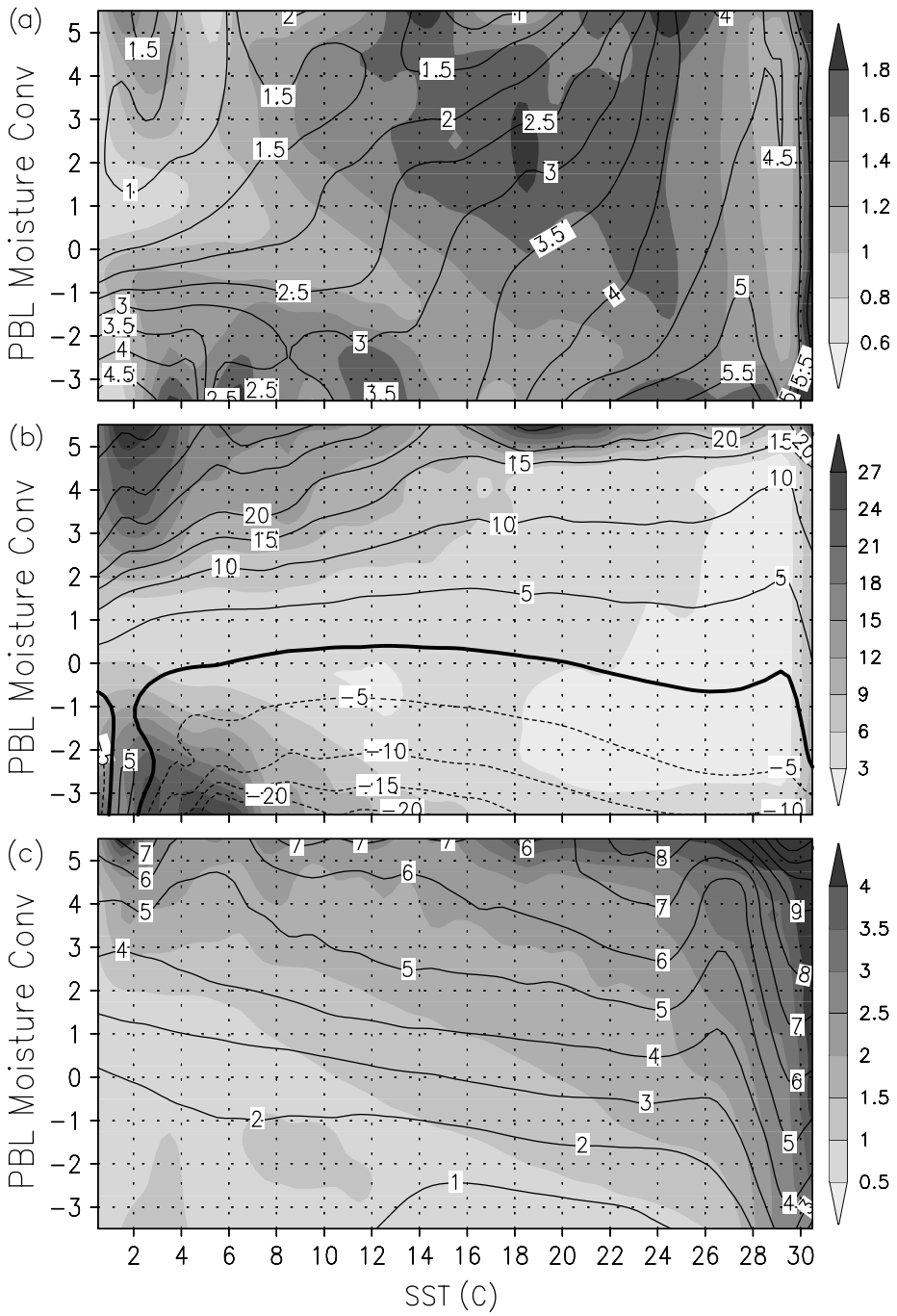

Figure 5. 10-year simulated fields (contours), binned by SST (1 °C bins) and BLqC: (a) surface evaporation, (b) PBL mass convergence, and (c) precipitation, all in mm d^{-1}. Shading (see key) denotes the standard deviation of the data in each bin.

distinguishing the SST-forced changes from the natural variability of the analyzed fields. Evidently, an isopleth of any analyzed field would reflect stronger dependence on BLqC (SST) if its orientation is more horizontal (vertical).

Figure 5(a) shows that, for SSTs below 10 °C, ocean evaporation corresponds more with BLqC and less with SST. For cold oceans, the influence of SST on saturation vapour pressure and/or saturation humidity is not as large as it is at high water temperatures. On the other hand, mixed-layer relative humidity is larger in ascent (or convergence) and smaller in descent (or divergence). Hence the humidity gradient for evaporation will be larger in descent and smaller in ascent. Naturally therefore, evaporation at latitudes of relatively lower SST correlates more with BLqC than with SST. Thus negative (positive) BLqC is associated with sinking (rising) and increased (reduced) evaporation, as seen in Figure 5(a). In the SST range 10–28 °C, the ocean evaporation shows marked increase with SST, but its increase with moisture divergence also remains valid up to about 20 °C. Above 20 °C, the dependence on moisture convergence/divergence dwindles, while the influence of SSTs starts to dominate as evidenced in the mostly vertical

orientation of the isopleths of evaporation. This relation supports the assumption that evaporation is proportional to the SST perturbations. Indeed, it will also hold for lower SSTs because the winds and PBL humidity are assumed to be unaffected by local SST perturbations. In our analysis, the assumption is used at the same grid point where everything else (including winds) remains the same.

Figure 5(b) shows horizontal orientation of BLmC isopleths. This reflects strong correspondence between BLqC and BLmC (also seen in Section 3); however, the dependence of BLmC on SSTs is reflected by the positive gradient of the isopleths with respect to the SSTs (mostly for lower SSTs and large convergence or divergence). Higher SSTs increase the moisture content of the PBL and that would require less BLmC for the same moisture removal by precipitation. Here again, for SSTs of 29 °C or more (for the same moisture convergence), the mass convergences or divergences decrease with SSTs and that implies higher humidity and smaller spatial humidity gradients, which indeed is true. The bin boxes at high SSTs represent a mix of regions; some regions are centres of high moisture convergence that are humid with precipitation, and others are of discernible moisture divergence (hot spots) with reduced precipitation. The bottom half of Figure 5(b) represents both negative BLqC and BLmC containing areas of large mass divergence associated with lower SSTs. The asymmetry in the patterns of moisture convergence and divergence regimes in regions of 0–10 °C SSTs is inconsequential for the present work and was not explored further. However, it is related to differences in the high and low pressure systems associated with mass and moisture convergence or divergence patterns.

Figure 5(c) shows isopleths of precipitation. For the same BLqC, the precipitation increases with SSTs because of increased oceanic evaporation. However, above 24–26 °C, the structure of isopleths of precipitation is quite unique. The precipitation, for the same moisture convergence, reduces with SST up to about 27 °C; these represent sinking regions around the ITCZ. In the SST range of 27–29 °C, there is a sharp increase in precipitation that reaches a maximum at around 29 °C and then starts to reduce again for still larger SSTs. Evidently, because of the arbitrary choice of an SST interval, the boundaries may not be precise, but the relationship of precipitation with respect to SST and moisture convergence is internally consistent. Why do we see less precipitation for the same moisture convergence above 29 °C? It occurs because the reduced evaporation in a shallow PBL together with moisture divergence above the mixed layer in the regions of hot spots leads to the reduction of averaged precipitation. Not all regions in the SST range 30 ± 1 °C and higher behave as above, but with a preponderance of such grid cells among the small number of all grid cells in the range 30 ± 1 °C, one notes a reduction in the averaged precipitation with SSTs. This also suggests how one can isolate the influence of SST perturbations in regions with externally forced large-scale circulation. If such regions experience large SST perturbations, only the local moist static energy of the PBL will be affected (Sud and Walker, 1999a), while the local moisture divergence may not be enough to make an impact on the thermodynamics of clouds and precipitation.

In the ITCZ regions, the precipitation is often less than the sum of the PBL moisture convergence and surface evaporation. The ratio defines the precipitation efficiency. In some areas, it gets close to 100% because moisture supply is enhanced by moisture-flux transports above the boundary layer (ignored in this analysis). In the coastal areas affected by the Andes, precipitation efficiency is very low. Here, we get warm and dry air intrusion that suppresses moist convection through dry entrainment.

4.6. Splitting precipitation by SST and PBL moisture convergence

We follow the methodology outlined in Section 3.2 to compute the partial derivatives of precipitation as a function of local SST. The effect of SST on local evaporation is implicit in the first term, whereas the effect of SST on moisture convergence was related primarily to BLqC defined by the second term in Equation (6). The partial derivatives are determined for the mean values of the doubly binned precipitation data shown in Figure 5(c). The two partial derivatives $\partial P/\partial T_{ss}$ and $\partial P/\partial M_b$ are computed along the abscissa and ordinate, respectively, of Figure 5(c). The term dM_b/dT_{ss} was computed from Equation (6). Equation (3) yields dP/dT_{ss} as $\partial P/\partial T_{ss}$ plus $\partial P/\partial M_b \times dM_b/dT_{ss}$. Results of these calculations are shown in Figure 6; the contours show that the rate of change of precipitation as a function of local SST is mainly the thermodynamic effect whereas the shaded background shows the influence of SST on precipitation due to change in PBL moisture convergence.

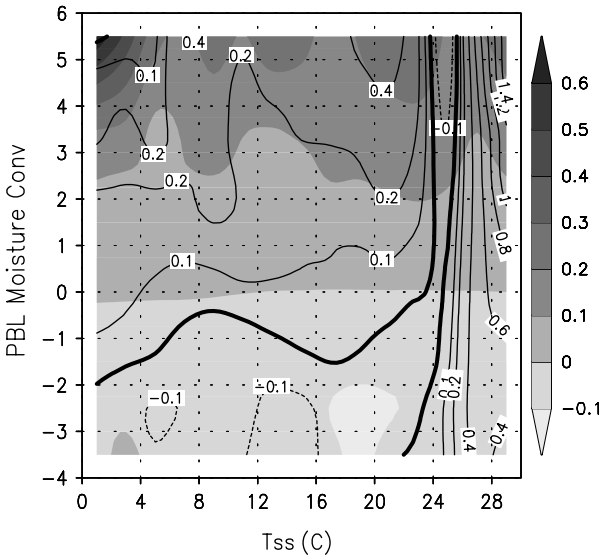

Figure 6. Model-simulated fields binned by SST and BLqC. Contours show dP/dT_{ss} (mm d^{-1} K^{-1}); shading (see key) shows $(\partial P/\partial M_b) \times (dM_b/dT_{ss})$, where M_b = BLqC.

Typically, $\partial P/\partial T_{ss}$ is mostly positive; however, if the SST increases and moistens the PBL, that in turn forces the PBL to mix its moisture into drier diverging air aloft; hence $\partial P/\partial T_{ss}$ can become negative, but not very often. Under those conditions, the vertical mixing helps the moisture to escape from the column atmosphere (the classical Sahara desert scenario in July when the moisture converging into the surface low escapes by mixing into the dry diverging air aloft; Sud and Molod, 1988). On the other hand, $\partial P/\partial Mb$ is almost always positive while dM_b/dT_{ss} is strongly positive in the Tropics and discernibly negative in regions of the subtropical high. In that case, the product will be negative in regions of moisture divergence.

The inferred quantity, dP/dT_{ss}, contains local SST contributions to precipitation by both the dynamic and thermodynamic effects. The analysis assumes linearity; hence there is a restriction on its application to small perturbations. The influence of SSTs on precipitation is large in the Tropics (SSTs between 26 and 30 °C). Here, the SST-induced evaporation and the near-surface moisture convergence work in concert to increase the precipitation. This is a well-known tropical phenomenon that led Bony *et al.* (1997) and several others to focus on the Tropics, seeking an SST–precipitation relationship. Interestingly, its dependence on PBL moisture convergence is not so critical for the overall outcome because the analysis is valid for small changes that do not materially modify the quasi-stationary circulation; the same outcome is evident in the verticality of the contours in Figure 6. The dP/dT_{ss} is as large as 1.4 mm d^{-1} C^{-1} at higher SSTs, which is supported by an increase in moisture convergence of only 0.4 mm d^{-1} C^{-1} in converging regions. This may appear counterintuitive, but recall that we are computing δT_{ss} influences at a single grid cell under the same mass convergence. Under strongly diverging conditions, dP/dT_{ss} is negative, particularly over SSTs lower than 22 °C, as seen in Figure 6. However, both partial derivatives are small in the diverging regions of the subtropics while the accompanying dM_b/dT_{ss} is negative. Thus their sum could be negative. In other words, small increases in SST can lead to a reduction in precipitation, an outcome consistent with Figure 2(b). Moreover the circulation is consistent with warm regions transporting moisture into the ITCZ or SPCZ regions. Howsoever small, this is a positive contribution of both SST and moisture convergence to precipitation except for highly subsiding regions. Some areas of $dP/dT_{ss} < 0$ imply that the increase in evaporation is mitigated by enhanced upward mixing of moisture that subsequently escapes with subsiding and diverging (often dry) air aloft. It represents the drying influence of shallow convection. In high-latitude low-SST regions, BLqC plus evaporation contributes to the majority of the precipitation, but with precipitation efficiency limits. Precipitation yields larger than 100% of BLqC plus evaporation imply moisture supply at the upper levels (neglecting humidity change of the PBL), which was evidenced in some regions (not shown).

4.7. Precipitation change due to SSTs

Figure 7 shows the projection of dP/dT_{ss} onto the global SST field for each of the four seasons. It illustrates how different oceanic domains are affected by local SST variations and moisture convergence on monthly to seasonal time-scales. The data were averaged over the entire 10-year simulation period, but separately for each season. In most warm regions, dP/dT_{ss} fields are positive. In the tropical regions they parallel the ITCZ. In March–April–May, we see a double ITCZ which is a consequence of the ITCZ being in the southern (northern) latitudes in the early (later) part of spring season. The transition involves its demise in the South Pacific and simultaneous emergence in the North Pacific (Goswami *et al.*, 1984) with the average giving the spurious appearance of a double ITCZ, but it does not happen every year because of the interannual variability of SSTs. SSTs also contribute to the shape of the ITCZ because the precipitation distribution around the ITCZ parallels the structure of the local SST. A similar picture of SSTs is seen in December–January–February climatology when there is only one ITCZ. This suggests the need to examine the local SST and all remote contributions to the total precipitation. Such an understanding can be useful for global change scenarios and even understanding the influence of sudden perturbations to the local SSTs in limited regions due to anthropogenic activity or other natural cataclysmic events.

4.8. Local SST-induced precipitation fraction

From Cs and Cc simulations and with the knowledge of dP/dT_{ss} at a location, we computed the influence on the local precipitation of interannual variations of the local SSTs. The dynamic contributions to precipitation change are simply the difference between the two. We produced monthly data of precipitation anomalies but will show the results of ten-year averages for each season. To estimate the significance of the SST influence on precipitation at any grid cell, we evaluated the simulated change against the natural variability of precipitation, σ_p, computed from the Cc simulations made with the 10-year mean SSTs that are devoid of the interannual SST variability. The precipitation anomaly budget relation is

$$\Delta P_t = \Delta P_l + \Delta P_r \pm \sigma_p. \tag{7}$$

Equation (7) shows that the total precipitation anomaly, ΔP_t, at any location (at the GCM grid-cell scale) consists of precipitation anomalies due to (i) local SSTs, as ΔP_l, plus (ii) all the remote influences, ΔP_r. Both of these are associated with an uncertainty due to σ_p. For n-year data with m months in each season, we recast Equation (7) as:

$$\frac{1}{nm}\left\{\sum_{nm}\left(\frac{\Delta P_l}{\Delta P_t}\right)+\sum_{nm}\left(\frac{\Delta P_r}{\Delta P_t}\right)\right\} \pm 2\frac{\sum_m \sigma_p n^{0.5}}{\sum_{nm}\Delta P_t} = 1, \tag{8}$$

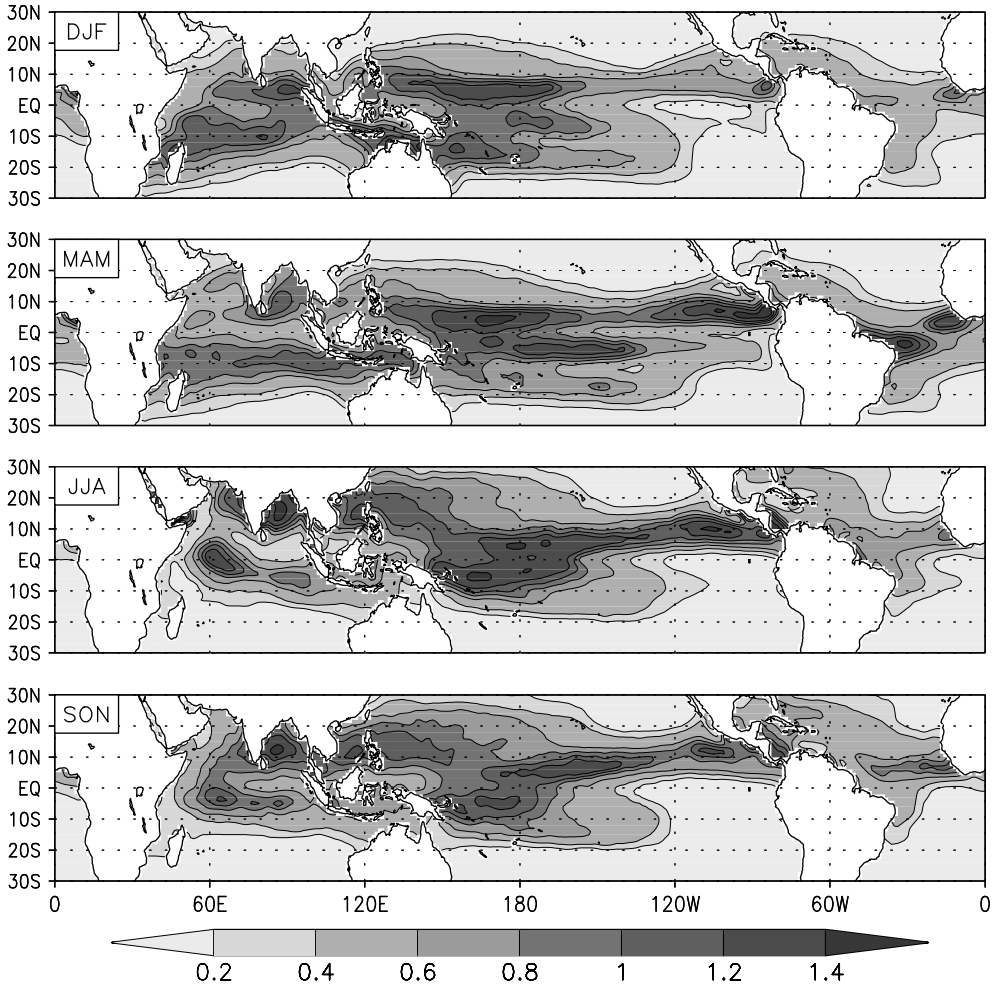

Figure 7. Seasonal mean dP/dT_{ss} (mm d^{-1} K^{-1}) averaged over 10 years in Cs simulation. Seasons are marked on each panel.

wherein all elements are scaled by total precipitation, ΔP_t and are averaged over n years and m months. The standard deviation divided by the sample size is the standard error, and twice the standard error,

$$\frac{2\sum_m \sigma_p \, n^{0.5}}{\sum_{nm} \Delta P_t},$$

yields the 95% confidence level.

Equation (8) can be used to examine the seasonal precipitation anomalies for La Niña SST anomaly year minus El Niño SST anomaly year for the same season (abbreviated as LME differences) as follows:

$$\frac{1}{m}\left\{\sum_m \frac{\Delta P_{l_{LME}}}{\Delta P_{t_{LME}}} + \sum_m \frac{\Delta P_{r_{LME}}}{\Delta P_{t_{LME}}}\right\} \pm \frac{2\sum_m \sigma_p}{\sqrt{2}\sum_m \Delta P_{t_{LME}}} = 1. \tag{9}$$

We used Cs and Cc simulations, one with naturally varying SSTs and one with prescribed SSTs (as described in Section 3.1), to infer the local (thermodynamic) versus all remote (dynamic) influences of SST fields on precipitation employing the monthly mean fields, and the above formulations were used to infer the statistical significance on the change determined from Equations (3)– (9).

Figure 8 shows the distribution of

$$\frac{1}{nm}\sum_{nm}\left(\frac{\Delta P_l}{\Delta P_t}\right)$$

over the global oceans for each of the four seasons. The local SST influence is larger in regions of higher SST. It has some contribution to a double ITCZ in March–April–May and a single ITCZ in the other three seasons. It shows the well-known dipole character in the tropical Atlantic in all seasons with the highest influence in the June–July–August period, when small changes in the local SSTs significantly affect the local precipitation and convective intensification. The influence of warm-pool and Indian Ocean SSTs on the local precipitation is small. This represents relatively smaller interannual variability of these SSTs with respect to the larger interannual variability of precipitation in these regions. It is large where the local fraction is small, but it can be a major contributor in the Tropics, particularly in regions where local SSTs do not change much. Indeed,

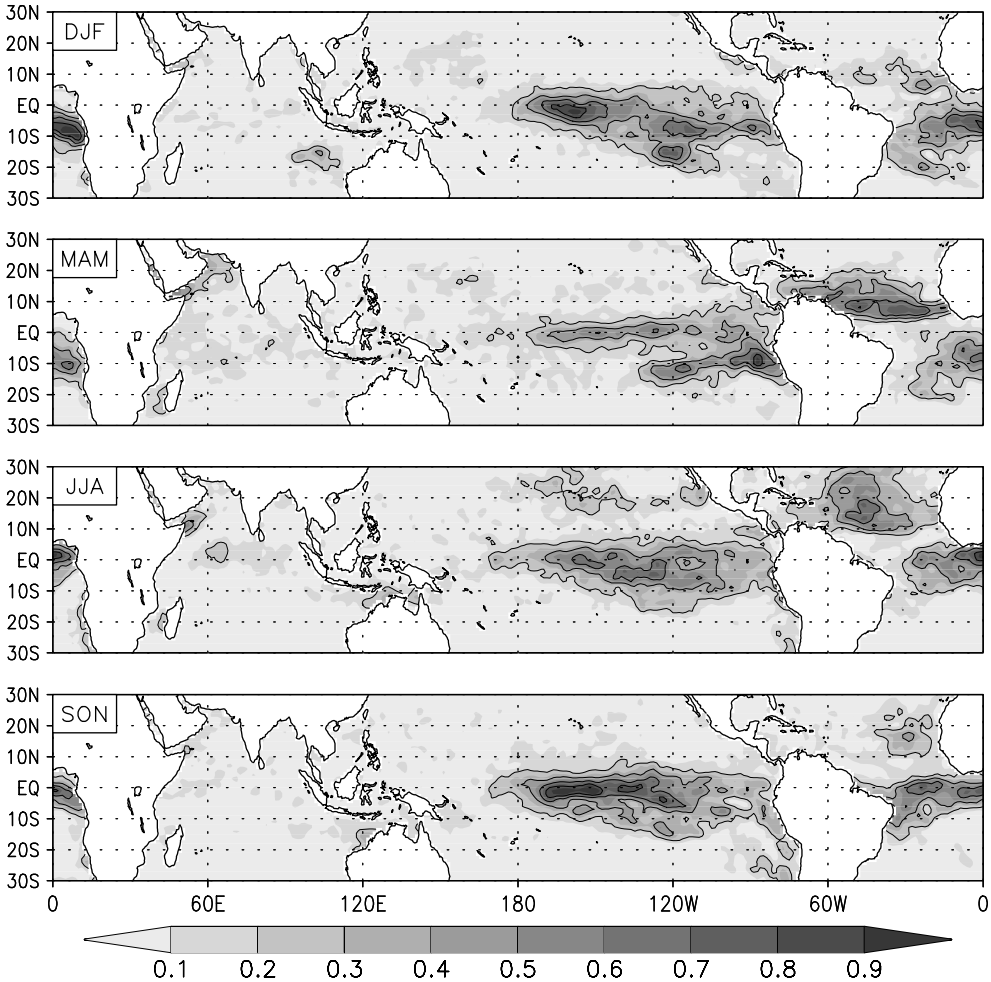

Figure 8. Seasonal mean rainfall variability as a fraction of the total rainfall variability in Cs simulation. Seasons are marked on each panel.

we will see later that the remote or dynamic contribution is significant almost everywhere.

4.9. Significance of local and remote SST contributions

The standard error of normalized precipitation in the 10-year ensemble (as defined in Section 4.8) is shown in Figure 9. Wherever twice the standard error is less than 0.5, at least one (either local or remote) SST influence is statistically significant at the 95% level. We find that the standard error over most of the grid cells is less than 0.25; accordingly most of the regions have a statistically significant response to one of the forcings. The calculation identified four types of region: (i) where the local SST influences were significant; (ii) where the large-scale SSTs and other remote influences were significant; (iii) where both influences were significant; and (iv) where natural variability was larger than both influences. Figure 10 shows very small areas where neither local nor remote effects are significant. Only the dark regions, found mostly in the Tropics, with large local SST–precipitation correspondence, show significant response to both local and remote SSTs. Outside of the dark regions, vast spans of Tropical and extratropical oceans show a remote response. Encapsulated within the dark regions, are small regions where the local SSTs have a predominant influence. This picture is much more revealing than those of the earlier studies and provides an unambiguous answer to the fundamental question of the influence of interannual SST changes on the local precipitation on monthly time-scales.

4.10. El Niño (1987) and La Niña (1988) SST-forced precipitation anomalies

One naturally wonders whether the analysis can distinguish between the responses of precipitation to local versus remote SST anomalies for precipitation differences corresponding to El Niño and La Niña years. Our integration period had only one such event. The result of this analysis is shown in Figure 11 wherein we again partition each grid cell into one of the four categories as outlined in Section 4.9. Even with huge local- as well as global-scale SST differences, the statistical significance of local versus global SST contributions (1987 minus 1988 differences) for one single case cannot be as significant as they would be for an ensemble of 10 cases (as seen in the 10-year data analysis). However, the methodology still holds. As expected, we find vast areas in which the differences are large but fail the statistical significance test.

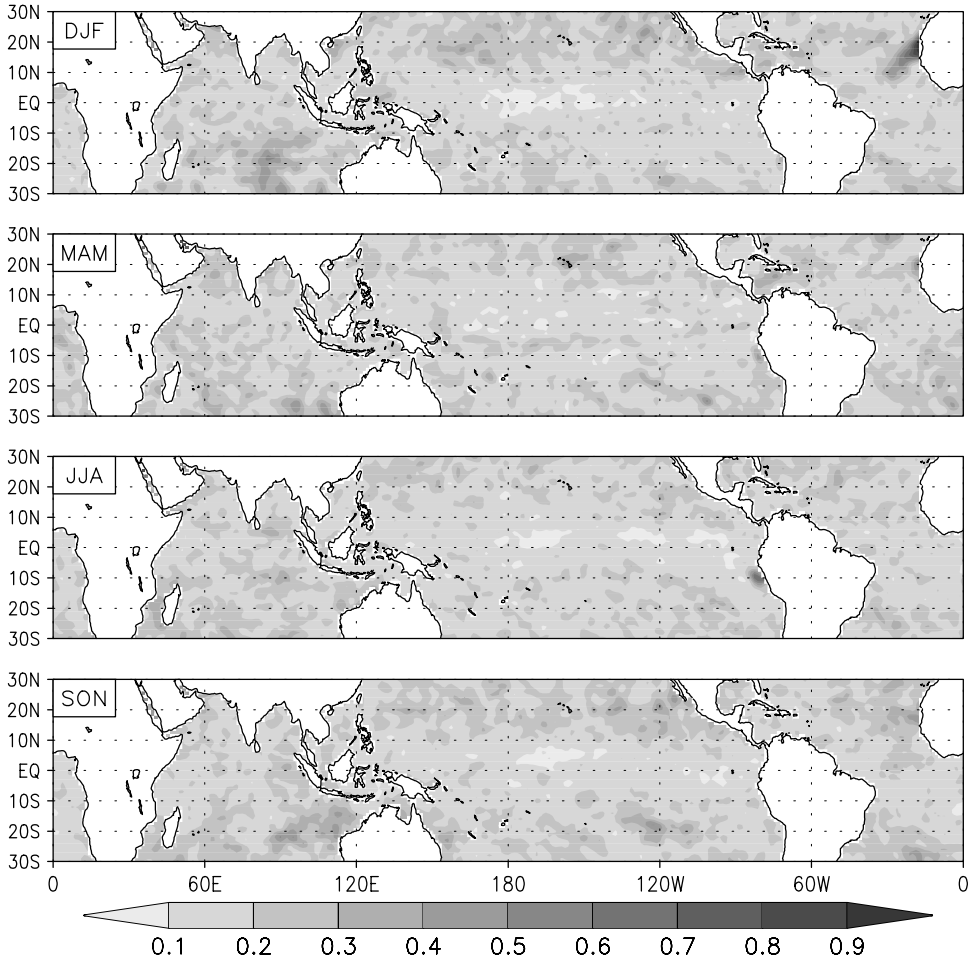

Figure 9. Seasonal mean standard error of rainfall in Cc simulation, shown as a fraction of the averaged total rainfall. Seasons are marked on each panel.

One can see some dark areas over regions of large SST anomalies in the Tropics and some grey areas at higher latitudes; however there are many more regions in which the precipitation anomalies fail the statistical significance test at the 95% confidence level.

5. Conclusions and summary

In the past, several investigators have explored the influence of local SST versus remote dynamics on the local precipitation. Since local SST and large-scale dynamics are interactive as well as intertwined, it is difficult to distinguish between them. Pioneering studies focused on the Tropics and resorted to binning and categorizing the data by SST and vertical velocity at 500 hPa (Bony *et al.*, 1997) and 200 hPa divergence (Lau *et al.*, 1997). Others have looked at the storm-scale physical processes (Del Genio and Kovari, 2002). We also followed the binning methodology, but then took a couple of extra steps to isolate the local and remote SST effects by invoking differential calculus for small SST perturbations and some reasonable physical assumptions. The new methodology is valid for the global domain, even though the major SST impacts only emerged in the Tropics, as expected.

Binning data by prudent selection of forcing functions sorts the data into similarly forced groups and averages out the influence of geographical juxtapositions of SSTs and/or PBL moisture convergences. This type of averaging is associated with uncertainty due to the physical assumptions and natural variability of the climate system. A straightforward binning by climatologically or naturally varying SSTs showed that: (i) averages of binned fields of evaporation, PBL moisture convergence, vertical velocity and precipitation are very similar for the two simulations, but both of them were enveloped by very similar but large standard deviations; (ii) the evaporation increased monotonically with SST up to about 27 °C before it plateaued with another sharp increase in the last bin 29–31 °C, (iii) the precipitation correlated much more with vertical velocity than with the local SST or evaporation; (iv) moisture convergence was largely associated with mass convergence as opposed to humidity gradients that are functions of SST gradients, and (v) the oceanic hot spots, small regions of high SSTs but reduced precipitation, are out of phase with SST-organized large-scale moisture convergence; consequently, they also emerge in the prescribed SST simulations.

We analytically derived that local precipitation changes are functions of change in evaporation and grid-scale

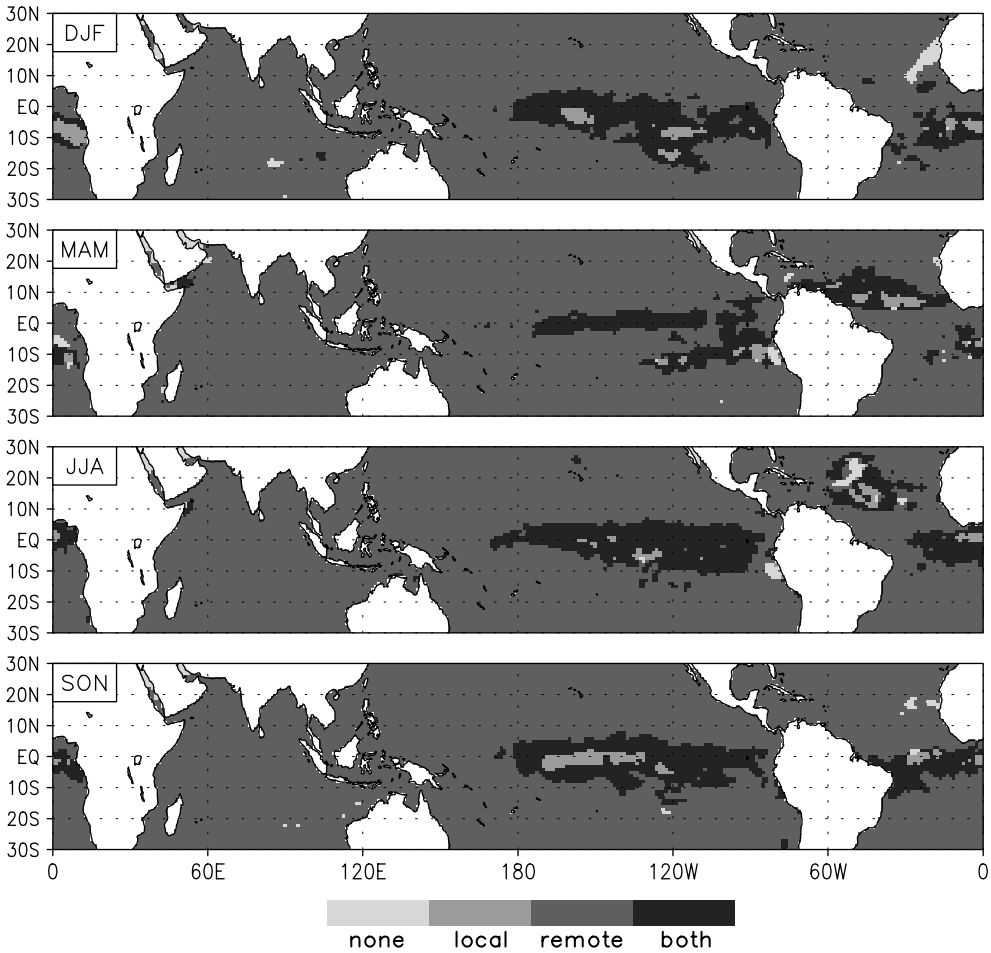

Figure 10. Distribution of interannual variations of precipitation (at ≥95% confidence level of statistical significance) in association with local and/or remote SST changes prescribed in the Cs simulation. Statistical significance of SST influences on precipitation are distinguished by four shades of grey (see key): none, local SST only, remote SSTs only, and both local and remote SSTs.

moisture flux convergence (or divergence) in the PBL, both of which are functions of the local SST. Using two 10-year monthly prescribed SST simulations, one using the analyzed SSTs with inter-annual variability and the other using its monthly means, we were able to obtain precipitation anomalies due to intra-annual SST variations along with the natural variability of precipitation from the climatological SST simulations. The changes of precipitation in response to local SST were estimated from changes in air-column thermodynamics of the grid cell plus the SST effects on moisture convergence within the PBL. The remote-SST effect was simply the total precipitation anomaly in the control (Cs) simulation minus the local-SST-induced precipitation anomaly ($= \{\mathrm{d}P/\mathrm{d}T_{\mathrm{ss}}\} \times \Delta T_{\mathrm{ss}}$). A comparison of the global distributions of the two fields revealed the influence of local and remote SST on precipitation.

The methodology needed doubly binned precipitation fields with respect to SST and PBL moisture convergence for determining partial derivatives of precipitation with SST and PBL moisture convergence. This together with $\mathrm{d}M_{\mathrm{b}}/\mathrm{d}T_{\mathrm{ss}}$ enabled us to compute the influence of local SST on precipitation at each grid cell. All other effects, including changes in far-field SSTs, soil moisture, and clouds, were lumped together as remote effects. The analysis helped to distinguish between the local SSTs and remote effects on precipitation anomalies over all oceanic grid cells. On projecting the influence of local SSTs on local precipitation, we extracted several useful insights. We found that the local-SST influence on the local precipitation was highest in the Tropics, but not everywhere. We also delineated regions with significant local- and/or remote-SST influences on precipitation. Clearly the analysis is valuable for climate change assessments and in deciphering the influence of SSTs on precipitation in different climatic regimes and seasons. Being physically derived, it has the potential of providing quantitative assessments of the consequences of small but realistic SST changes on precipitation.

We reiterate two main limitations of the methodology. First, if SST changes are large and alter significantly the mean monthly structure of the large-scale circulation, the linear analysis involving partial derivatives becomes inapplicable. Second, the use of fvGCM2 data warrants the usual cautions about the limitations of model-simulated data. The value of our findings is

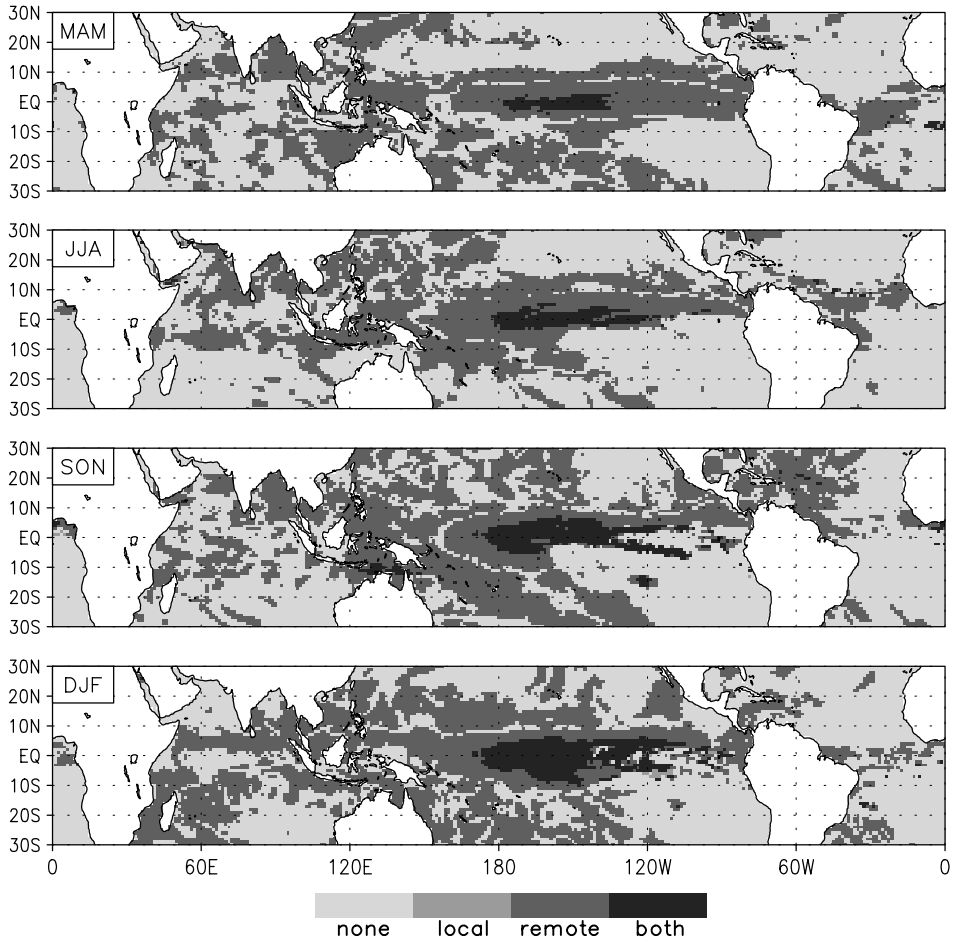

Figure 11. Statistical significance of the 1988 minus 1987 precipitation fields simulated in Cs. Shading for statistical significance is as in Figure 10, but the panels are arranged differently.

limited by the model's ability to simulate realistically the annual cycle of circulation and precipitation. Moreover, GCM simulations using the prescribed SSTs do not allow two-way air–sea coupling, in which SSTs are also modulated by the atmosphere and this can be significant (Seager *et al*., 2003); such a coupling has been shown to exert beneficial influences on tropical forecasts (e.g. Wang *et al*., 2005). Nevertheless, how the prescribed SST simulations affect the statistics of 10-year circulation and precipitation climatology (and our inferences) was not addressed. It depends upon the model's systematic biases that interact with and/or react to the observed SSTs. We hope to reassess these findings using simulations performed with a coupled ocean–atmosphere model. We would also like to re-examine the inferences using the analyzed data as soon as the analysis systems can provide observational-quality precipitation fields and moisture fluxes, which is becoming a distinct possibility (Max Suarez 2007, personal communication).

Acknowledgements

We thank both anonymous reviewers for valuable comments and recommendations to better clarify the concepts and ideas of our analysis and how prescribed SST simulations relate to observations. The authors also wish to thank Professors P. Read and R. Seager for several useful comments on the original manuscript. NASA HQ funding managers Dr. Don Anderson and Dr. Tsengdar Lee supported our research and provided computer resources. Participation of YCS, WK-ML, and GKW is the result of that support. YPZ is supported by NASA Earth Science Enterprise's Multidisciplinary Research in Climate, Chemistry, and Global Modeling.

References

Betts AK, Ball JH, Bosilovich M, Viterbo P, Zhang Y, Rossow WB. 2003. Intercomparison of water and energy budgets for five Mississippi sub-basins between ECMWF reanalysis (ERA-40) and NASA Data Assimilation Office fvGCM for 1990–1999. *J. Geophys. Res.* **108**: DOI: 10.1029/2002JD003127.

Bony S, Lau KM, Sud Y. 1997. Sea surface temperature and large-scale circulation influences on tropical greenhouse effect and cloud radiative forcing. *J. Climate* **10**: 2055–2077.

Cayan DR. 1992. Latent and sensible heat flux anomalies over Northern Oceans: The connection to monthly atmospheric circulation. *J. Climate* **5**: 354–369.

Chang Y, Schubert SD, Lin S-J, Nabuda S, Shen B-W. 2001. The climate of FVCCM-3 model. NASA/TM 104606, **20**: Ed: M. J. Suarez. Technical Report Series on Global Modeling and Data Assimilation.

Chen C. 2005. Relative impact of local and remote SST forcing on the climate predictability. *Geophys. Res. Abstracts* **7**: 02869.

Chou M-D, Suarez MJ. 1994. An efficient thermal infrared radiation parameterization for use in general circulation models. NASA/TM

104606, **3**: Technical Report Series on Global Modeling and Data Assimilation.

Chou M-D, Suarez MJ, Ho C-H, Yan M-H, Lee K-T. 1998. Parameterizations for cloud overlapping and shortwave single scattering properties for use in general circulation and cloud ensemble models. *J. Climate* **11**: 202–214.

Chou M-D, Lee K-T, Tsay S-C, Fu Q. 1999. Parameterization of cloud longwave scattering for use in atmospheric models. *J. Climate* **12**: 159–169.

Chou M-D, Chou S-H, Chan P-K. 2005. Influence of transient atmospheric circulation on the surface heating of the western Pacific warm pool. *Geophys. Res. Lett.* **32**: L08750, DOI: 10.1029/2005GL022359.

Del Genio AD, Kovari W. 2002. Climatic properties of tropical precipitating convection under varying environmental conditions. *J. Climate* **18**: 2597–2615.

Del Genio AD, Yao MS, Kovari W, Lo KKW. 1996. A prognostic cloud water parameterization for global climate models. *J. Climate* **9**: 270–304.

Fu X, Wang B, Waliser DE, Tao L. 2007. Impact of atmosphere-ocean coupling on the predictability of monsoon intraseasonal oscillations. *J. Atmos. Sci.* **64**: 157–174.

Giannini A, Chiang JCH, Cane MA, Kushnir Y, Seager R. 2001. The ENSO teleconnection to the tropical Atlantic ocean: Contributions of the remote and local SSTs to rainfall variability in the tropical Americas. *J. Climate* **14**: 4530–4544.

Goswami BN, Shukla J, Schneider EK, Sud YC. 1984. Study of the dynamics on the intertropical convergence zone with a symmetric version of the GLAS climate model. *J. Atmos. Sci.* **41**: 5–19.

Gushchina D, Dewitte B, Illig S. 2006. Remote ENSO forcing versus local air-sea interaction in QTCM: A sensitivity study to intraseasonal variability. *Adv. Geosci.* **6**: 289–297.

Harrison DE, Craig AP. 1993. Ocean model studies of the upper ocean variability at at 0°N, 160°W during the 1982–1983 ENSO: Local and remotely forced response. *J. Phys. Oceanogr.* **23**: 426–451.

Huffman GJ, Adler RF, Arkin P, Chang A, Ferraro R, Gruber A, Janowiak J, McNab A, Rudolf B, Schneider U. 1997. The Global Precipitation Climatology Project (GPCP) combined precipitation dataset. *Bull. Am. Meteorol. Soc.* **78**: 5–20.

Hurrell JW, Hack JJ, Boville BA, Williamson DL, Kiehl JT. 1998. The dynamical simulation of the NCAR Community Climate Model version 3 (CCM3). *J. Climate* **11**: 1207–1236.

Kim MK, Lau KM, Chin M, Kim KM, Sud YC, Walker G. 2006. Atmospheric teleconnection over Eurasia induced by aerosol radiative forcing during boreal spring. *J. Climate* **19**: 4700–4718.

Koster RD, Dirmeyer PA, Guo Z, Bonan G, Chan E, Cox P, Gordon CT, Kanae S, Kowalczyk E, Lawrence D, Liu P, Lu C-H, Malyshev S, McAvaney B, Mitchell K, Mocko D, Oki T, Oleson K, Pitman A, Sud YC, Taylor CM, Verseghy D, Vasic R, Xue Y, Yamada T. 2004. Regions of strong coupling between soil moisture and precipitation. *Science* **305**(5687): 1138–1140.

Larson K, Hartmann DL. 2003a. Interactions among cloud, water vapor, radiation and large-scale circulation in the tropical climate, Part 1: Sensitivity to uniform sea surface temperature changes. *J. Climate* **16**: 1425–1440.

Larson K, Hartmann DL. 2003b. Interactions among cloud, water vapor, radiation and large-scale circulation in the tropical climate, Part 2: Sensitivity to spatial gradients of sea surface temperature. *J. Climate* **16**: 1441–1455.

Lau KM, Wu HT, Bony S. 1997. The role of large-scale atmospheric circulation in the relationship between tropical convection and sea surface temperature. *J. Climate* **10**: 381–392.

Lohmann A, Krauss A, Hinrichsen H-H. 2002. Effects of remote and local atmospheric forcing on circulation and upwelling in the Baltic Sea. *Tellus* **A 54**: 299–361.

Lin S-J. 2004. A 'vertically Lagrangian' finite-volume dynamical core for global models. *Mon. Weather Rev.* **132**: 2293–2307.

Lin S-J, Rood RB. 1996. Multidimensional flux-form semi-Lagrangian transport schemes. *Mon. Weather Rev.* **124**: 2046–2070.

Lin B, Wielicki BA, Minnis P, Chambers L, Xu K-M, Hu Y, Fan A. 2006. The effect of environmental conditions on tropical deep convective systems observed from the TRMM satellite. *J. Climate* **19**: 5745–5761.

Maloney ED. 2002. An intraseasonal oscillation composite lifecycle in the NCAR CCM3.6 with modified convection. *J. Climate* **15**: 964–982.

Maloney ED, Hartmann DL. 2001. The sensitivity of intraseasonal variability in the NCAR CCM3 to changes in convective parameterization. *J. Climate* **14**: 2015–2034.

Moorthi S, Suarez MJ. 1992. Relaxed Arakawa-Schubert: A parameterization of moist convection for general circulation models. *Mon. Weather Rev.* **120**: 978–1002.

Peña M, Cai M, Kalnay E. 2004. Life span of subseasonal coupled anomalies. *J. Climate* **17**: 1597–1604.

Rayner NA, Parker DE, Horton EB, Folland CK, Alexander LV, Rowell DP, Kent EC, Kaplan A. 2002. Global analyses of sea surface temperature, sea ice, and night marine air temperature since the late nineteenth century. *J. Geophys. Res.* **108**(D14): 4407, DOI: 10.1029/2002JD002670.

Rind D, Rossow W. 1984. The effect of physical processes on Hadley Circulation. *J. Atmos. Sci.* **41**: 479–507.

Seager R, Murtugudde R, Clement A, Herweijer C. 2003. Why is there an evaporation minimum at the Equator? *J. Climate* **16**: 3793–3802.

Su H, Neelin JD. 2002. Teleconnection mechanisms for tropical Pacific descent anomalies during El Niño. *J. Atmos. Sci.* **59**: 2682–2700.

Su H, Neelin JD, Chou C. 2001. Tropical teleconnection and local response to SST anomalies during the 1997–1998 El Niño. *J. Geophys. Res.* **106**(D17).

Sud YC, Molod A. 1988. The roles of dry convection, cloud-radiation feedback processes and the influence of recent improvements in the parameterization of convection in the GLA GCM. *Mon. Weather Rev.* **116**: 2366–2387.

Sud YC, Walker GK. 1999a. Microphysics of clouds with the Relaxed Arakawa-Schubert Scheme (McRAS). Part I: Design and evaluation with GATE Phase III data. *J. Atmos. Sci.* **56**: 3196–3220.

Sud YC, Walker GK. 1999b. Microphysics of clouds with the Relaxed Arakawa-Schubert Scheme (McRAS). Part II: Implementation and performance in GEOS II GCM. *J. Atmos. Sci.* **56**: 3221–3240.

Sud YC, Walker GK. 2003. Influence of ice-phase physics of hydrometeors on moist-convection. *Geophys. Res. Lett.* **30**: 1758, DOI: 10.1029/2003GL017587.

Sud YC, Walker GK, Lau K-M. 1999. Mechanisms regulating sea-surface temperatures and deep convection in the tropics. *Geophys. Res. Lett.* **26**: 1019–1022.

Sud YC, Mocko DM, Lin S-J. 2006. Performance of two cloud-radiation parameterization schemes in the finite volume general circulation model for anomalously wet May and June 2003 over the continental United States and Amazonia. *J. Geophys. Res.* **111**: D06201, DOI: 10.1029/2005JD006246.

Sundqvist H, Berge E, Kristjänsson JE. 1989. Condensation and cloud parameterization studies with a mesoscale numerical weather prediction model. *Mon. Weather Rev.* **117**: 1641–1657.

Tiedtke M. 1993. Representation of clouds in large-scale models. *Mon. Weather Rev.* **121**: 3040–3061.

Waliser DE. 1996. Formation and limiting mechanisms for very high sea surface temperature: Linking the dynamics and thermodynamics. *J. Climate* **9**: 161–188.

Wang B, Ding Q, Kang I-S, Shukla J, Jin E, Fu X, Doblas-Reyes F. 2005. Fundamental challenge in simulation and prediction of summer monsoon rainfall. *Geophys. Res. Lett.* **32**: L15711, DOI: 10.1029/2005GL022734.

Yu L, O'Brien J, Yang J. 1991. On the remote forcing of the circulation in the Bay of Bengal. *J. Geophys. Res.* **96**: 20449–20454.

Zhang C. 1993. Large-scale variability of atmospheric deep convection in relation to sea surface temperature in the Tropics. *J. Climate* **6**: 1898–1913.